VLBA Sensitivity Upgrade Memo 45

Testing the Goddard Calc 11 Delay Model at the VLBA

W. Max-Moerbeck[1,2] and W. Brisken[1]

ABSTRACT

We describe the results of a series of tests designed to verify the performance of a new delay model, Calc 11. This new delay model is compared with the current delay model implementation Calc 9, which is also used as a base level for performance. We perform tests to exercise the delay models with sources at different elevations, and also to compare their performance in two simple phase-referencing experiments, one using bright calibrator sources and another observing Mars orbiters which also test the implementation of near-field effects.

1. Introduction

The delay model is an essential component for any very long baseline interferometer, and in particular for the DiFX correlator used in the VLBA (Deller et al. 2007). It is used to align in time the data from two different antennas at an specific point on space usually the geocenter. This geometric delay, $\tau(t)$, depends on the position of the stations and time and it includes the geometry of the Earth, incorporating the effect of ocean and atmospheric loading, as well as its rotation. The currently used model, Calc 9.1, was released in 1999 and has been used at the VLBA since then, preceded by Calc 9.0 used since 1995. The current version of the delay model, Calc 11 is still in a period of final development, and it incorporates a few key improvements that we would like to have in the DiFX correlator for the VLBA such as:

- It can run as a stand-alone executable that is well integrated with DiFX.
- Antenna tilts are incorporated (important for Pie Town).
- Several features previously tacked onto Calc in the "calcserver" program are now integral to Calc such as near field delay model, and ocean loading.

This memo describes the tests we made to verify the performance of our implementation of Calc 11, and its integration within the DiFX correlator. Given the complexity of this system we took an empirical, data-driven approach to verify that Calc 11 produced comparable results as Calc 9, and determine the conditions under which possible discrepancies could be found. To this end, we compared the predicted geometric delays as directly returned by each Calc model and their residuals as determined by fringe fitting in AIPS for a series of astronomical

[1]National Radio Astronomy Observatory, Socorro, NM

[2]Max Planck Institute for Radio Astronomy, Bonn, Germany

observations. We also verify their effect on two phase-referencing experiments, one using bright calibrator sources and one observing Mars orbiters which also test the implementation of near-field effects.

2. Observations and data reduction

Three sets of observations were used in this investigation, which are described below. In the first two cases we observed simultaneously in the S and X-bands, using the standard setup for the USNO UT1-UTC daily measurements. The Mars orbiter tests use 2 IFs of 32 MHz in the X-band centered[1] at 8406.851853 MHz and 8439.444446 MHz, with channels of 50 kHz. This is required by the narrow band nature of the spacecraft down-link signals.

TV010A: In this test we observed a group of 11 sources taken from the list of VLBA calibrators. Three of them were used to perform a phase referencing experiment, these are J2216+3518, J2212+3308 and J2203+3145, all a few degrees away of each other. The other 8 sources were chosen to be at a range of elevations, to test a possible dependence in the performance of the delay models with elevation. The data reduction was performed using standard procedures in AIPS, including flagging of periods with anomalous system temperatures, and the complete excision of the two most extreme IFs in the S-band due to RFI contamination.

BF115 series: This test was commissioned by the USNO to study precision of Earth orientation measurements made with 5 VLBA antennas. We use 16 epochs of these tests[2], in which sources at different sky positions are observed, thus providing data for the comparison of the delay models under different conditions. Each of the 16 epochs was flagged for anomalous system temperatures, plus the excision of the two most extreme S-band IFs as for TV010A.

TS036C: In this test observations of the Mars orbiters Mars Reconnaissance Orbiter (MRO) and Odyssey are included. The observations are an hour long and include data on a fringe finder source (3C 454.3) and two phase calibrators close to Mars position at the time of the observations (J2259−0811 and J2306−0459).

3. Comparison of the raw delays from each delay model

Calc 9 and Calc 11 were used to compute delay models for experiment TV010A. Here we examine the model differences. Figures 1 and 2, and their captions illuminate the major differences. Absolute differences in delay model up to 70 ps (corresponding to about 1.5 turns phase at X-band) were seen. Extrapolation hints that differences up to a factor of two more are likely. Ignoring an anomaly at PT (see Fig. 2), the phase-referencing sections hint that for separations of $\sim$4.5 deg difference-of-model-differences are up to 6 ps. Much of this is common-mode (e.g., similar double-difference seen at multiple antennas), however the residual differences could still allow relative astrometry over the 4.5 degree angle on the sky to approach the 10 μas level. See Sec. 5 for experimental evaluation of this.

[1] In practice the center frequency is the closest 0.25 MHz point of the Doppler-shifted received frequency

[2] Tests BF115Y to BF115ZO are included

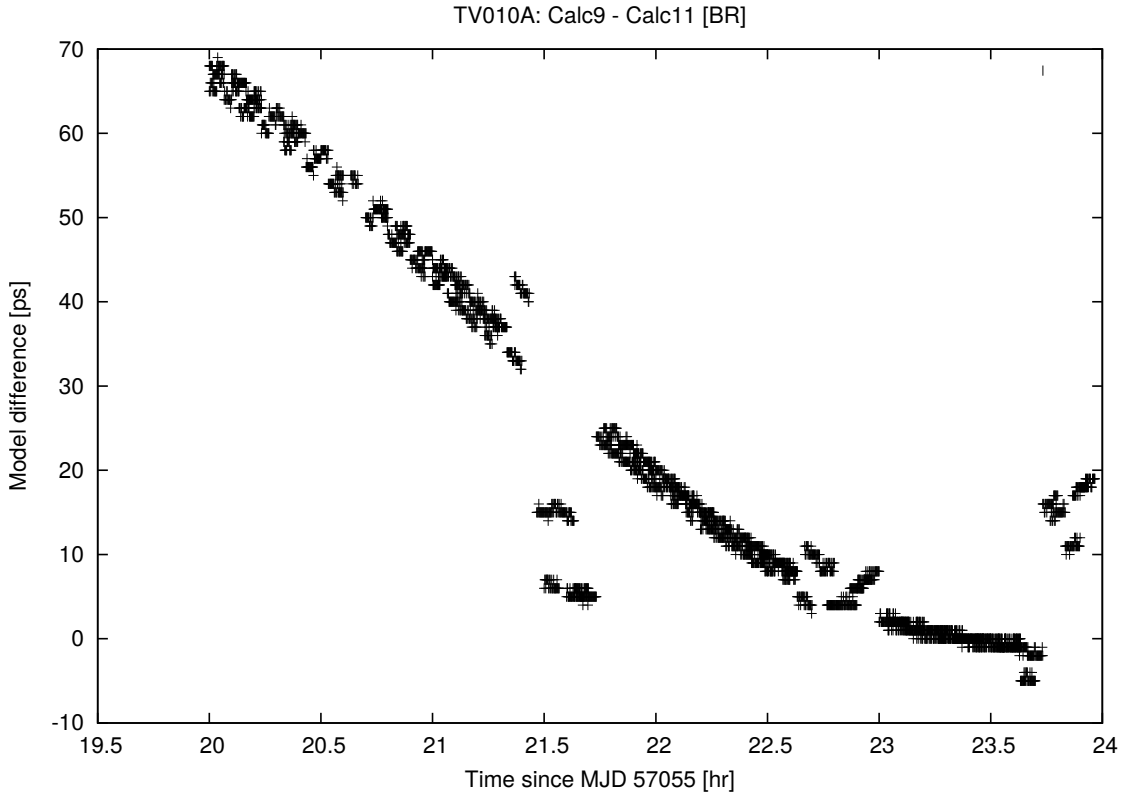

Fig. 1.— The difference between the delay model calculated by Calc 9 and Calc 11 for antenna BR in test experiment TV010A. Of all stations in this test BR exhibited the largest difference between the models at 70 ps. Structure from the two observing modes are clearly seen: the phase-referencing sections are seen as three tracks (one for each source) well approximated by portions of sinusoids of 24 hour period. Extrapolating these sinusoids suggest that a peak model difference of about 140 ps is likely for sources at declinations between 31 and 35 degrees. Interrupting this sequence are three sections where several sources across the sky are observed.

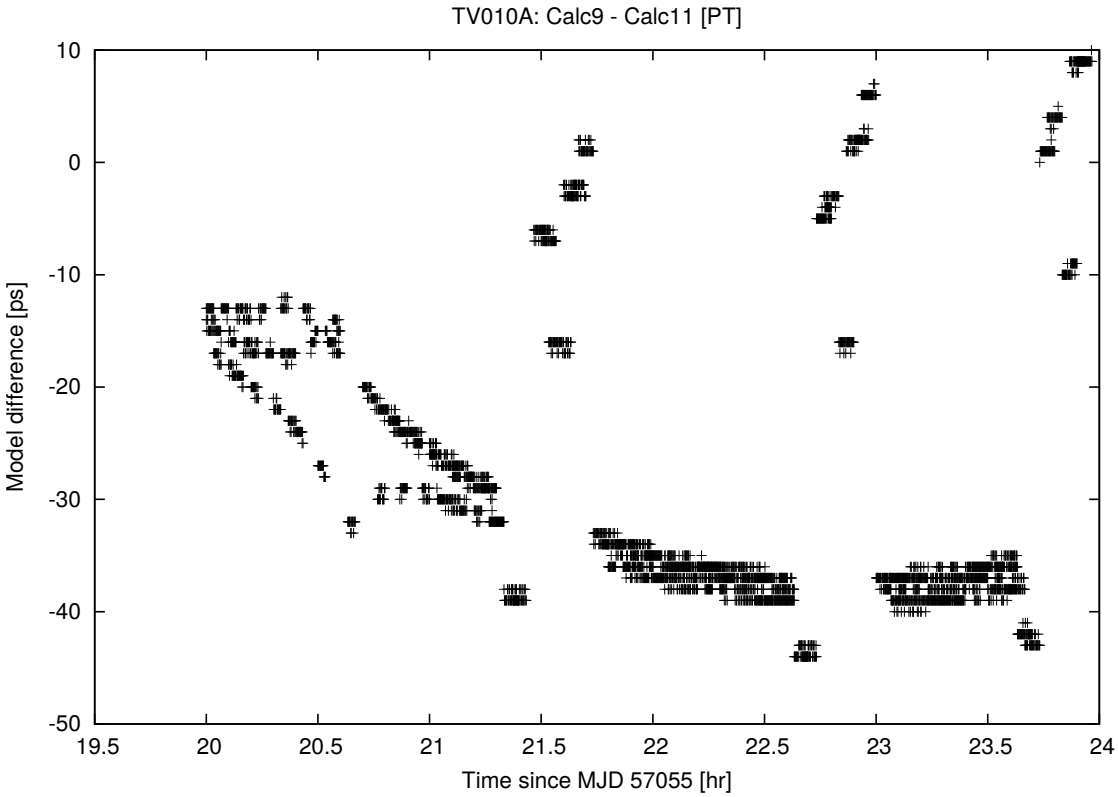

Fig. 2.— Same as Fig. 1 but for PT. This antenna exhibited the most dramatic Calc 9 vs. Calc 11 model differences. The triplet of sources included in the phase-referencing portion (J2203+3145, J2212+3308 and J2216+3518) transit PT between 2015 and 2030 UT. Owing to the latitude of PT (34.3 deg), the first two sources transit to the south and the third transits to the north. Calc 11 now includes modeling of the tilt of PT which may be responsible for the additional model differences seen between 2000 and 2100 UT on top of the 24-hour sinusoid.

4. All sky comparison of the two delay models

In the all-sky comparison we measure the residual delay correction using the FRING task in AIPS, for sources at various sky positions. An independent residual delay is estimated for each IF in the S-band and X-band. These residual delays will have a large component (specially the S-band ones) coming from the ionosphere which is not modeled in Calc. The ionospheric contribution has a well defined frequency dependence that can be modeled and cancelled by using pairs of IFs, thus providing an ionospheric free residual delay measurement as described below.

Let us take a delay δ_1 at frequency ν_1 and δ_2 at frequency ν_2. The delay at each frequency is composed of non modeled components that can be frequency independent (e.g., geometric and atmospheric errors) and frequency dependent as ionospheric dispersion which scale as ν^{-2}, so we can write the delays as

$$\delta_1 = \delta_{\rm ion\,free} + \delta_{0,\,\rm ion}\,\nu_0^2/\nu_1^2 \quad (1)$$

$$\delta_2 = \delta_{\rm ion\,free} + \delta_{0,\,\rm ion}\,\nu_0^2/\nu_2^2, \quad (2)$$

where $\delta_{\rm ion\,free}$ is the ionosphere free delay component, and $\delta_{0,\,\rm ion}$ is the ionospheric dependent delay at a reference frequency ν_0. $\delta_{\rm ion\,free}$ can be obtained by combining the equations above as

$$\delta_{\rm ion\,free} = \frac{\delta_1\nu_1^2 - \delta_2\nu_2^2}{\nu_1^2 - \nu_2^2}. \quad (3)$$

For a given baseline and scan, we can obtain an ionosphere-free delay estimate for each pair of IFs. We chose to use one in the S-band and one in the X-band to have a wider frequency separation, thus increasing the magnitude of the differential ionospheric effect. We produce an estimated residual ionosphere free delay for each scan in a baseline by taking the average of all the S-band/X-band IF pairs. We can then obtain a series of residual ionosphere free delays for each scan in a given baseline, which under ideal conditions should all be the same. In practice the delay model is not perfect as there are residual calibration errors associated with unmodeled atmospheric and ionospheric effects. To quantify the difference to this ideal case, we measure for each baseline the RMS of the deviations to the average value, and use this as a single number characterizing the quality of the delay model in the given baseline. We call this the ***baseline delay mean*** and ***baseline delay RMS***. We also compute the mean value of the RMS for all the baselines, thus getting a single value for an experiment, which we call the ***array delay RMS***.

4.1. BF115 series

This series of tests[3] uses 5 VLBA stations to perform geodetic type observations by looking at bright sources at different sky positions. We have data correlated with two delay models for 16 epochs, that are each analyzed as described above.

In computing the ionosphere free delays we found that some scans for a given baseline produced largely discrepant delays, thus affecting our comparison metric based on the baseline delay RMS of those delays. By

[3]This test series was commissioned by USNO to study precision of Earth orientation measurements made with 5 VLBA antennas.

examining some of these cases it was noticed that many of them happened when only a few IFs have valid solutions, usually in the X-band. It was also noticed that in some cases a single discrepant delay was produced by a single IF that had a low SNR for the delay. To filter out those cases we set thresholds for the minimum number of IFs pairs and minimum SNR. The used thresholds are a minimum of 21 IF pairs, of a total of 40 IF pairs that result from 4 IFs in the S-band and 10 IFs in the X-band. For the signal-to-noise ratio we use a minimum of 30. No attempt to choose optimal thresholds was made, and these values were selected just to get rid of the discrepant delays, and they are certainly filtering good cases. Even though we are loosing good measurement by this procedure, we are not flagging based on the quantity we are trying to estimate, as it would be the case if we were just removing discrepant points directly, so no significant biases in the baseline and array delay RMS estimates are expected. As for the cause of the discrepant data points, they seem to be related to low flux density compared to the noise in the observations, in particular in the X-band.

Figure 3 shows a summary of the results for BF115ZC which has data in all five antennas, while Figure 4 shows a summary of the delay RMS results for all the epochs combined.

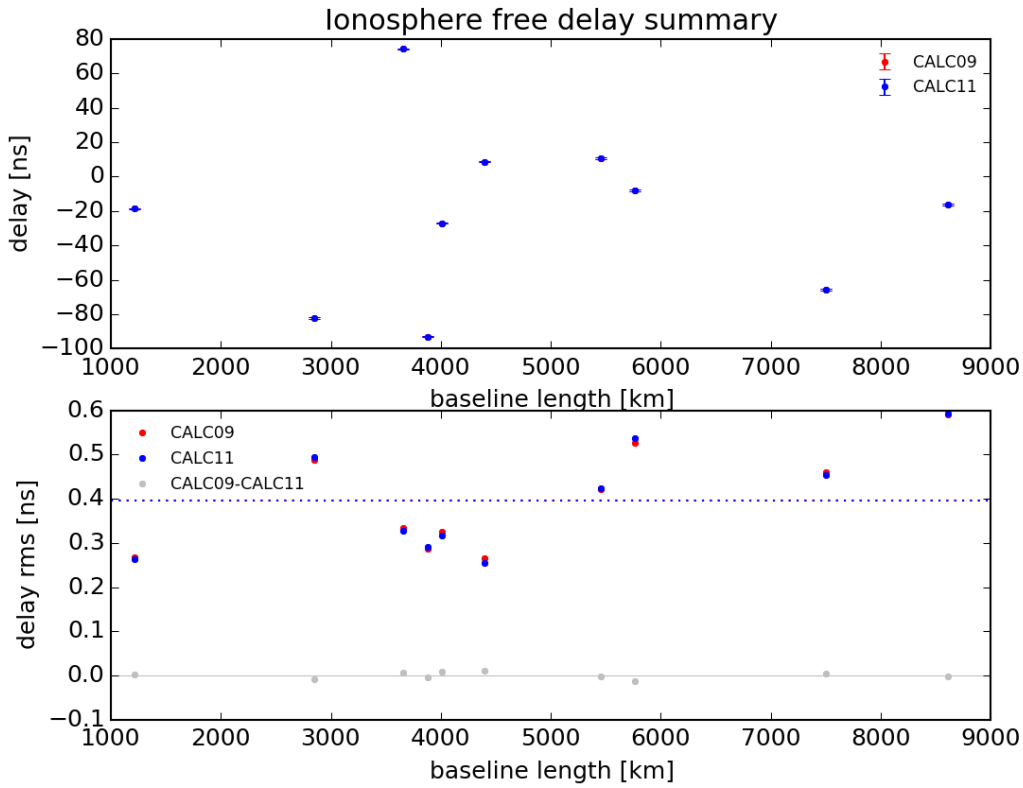

Fig. 3.— Residual baseline delay mean and RMS for each baseline, as a function of baseline length, for experiment BF115ZC. Upper panel: Residual baseline delay mean. Both models have consistent results. Lower panel: Residual beaseline delay RMS. Red dots are for Calc 9, blue for Calc 11, and grey for the difference. There are small differences, and no preference for a particular delay model is seen here. The array delay RMS for this test is 0.3966 ns for Calc 9 (red dotted line) and 0.3959 ns for Calc 11 (blue dotted line).

Figure 4 shows that the difference between the models is small, of only −1.7 ps for the difference of the array delay RMS (Calc 9-Calc 11).

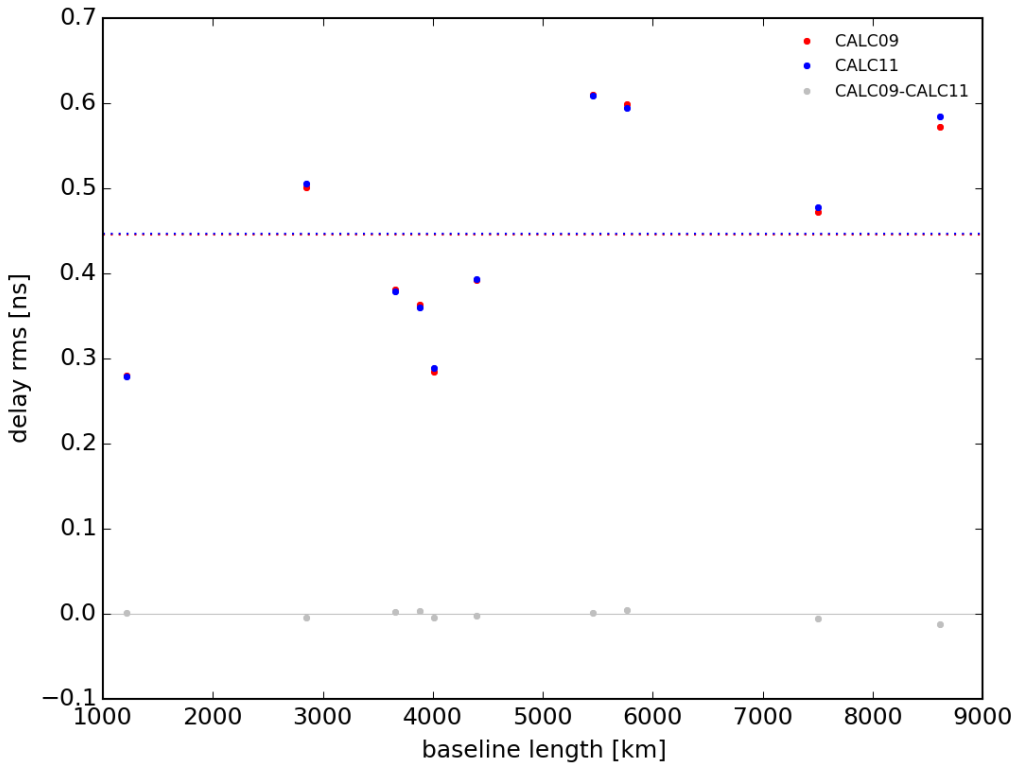

Fig. 4.— Average value for all the experiments of the residual baseline delay RMS for each baseline as a function of baseline length. The symbols are as for Figure 3. As in that figure, the differences between the delay models are small and show no preference for any of them. The array delay RMS for the 16 tests combined is 0.4455 ns for Calc 9 and 0.4472 ns for Calc 11.

4.2. TV010A

In this test we observe bright calibrators at different elevations and perform a phase-referencing experiment to verify the performance of the two delay models under the conditions of a real astronomical observation. In this section we present the results of the residual baseline and array delay RMS. The results for the phase-referencing part are presented in Section 5. We use the same data selection criteria described in 4.1.

Figure 5 shows the results for the delay RMS for each baseline. The array delay RMS for the experiment is is 0.3802 ns for Calc 9 and 0.3829 ns for Calc 11.

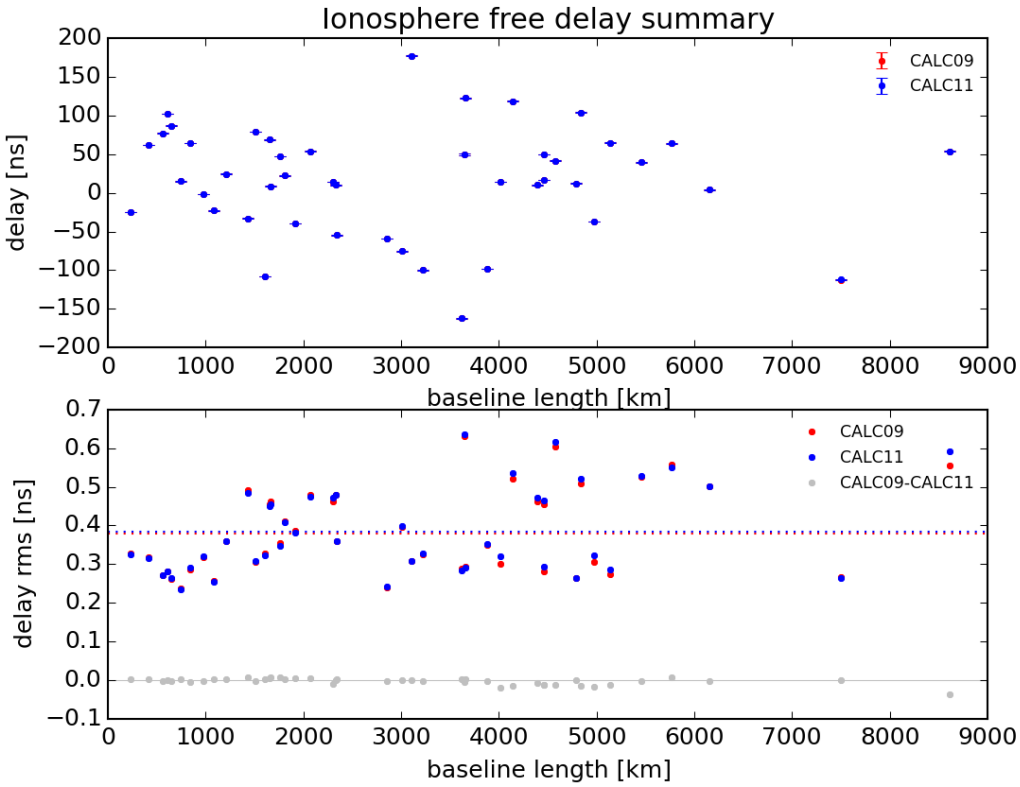

Fig. 5.— Residual baseline delay mean and RMS for each baseline, as a function of baseline length, for experiment TV010A. Upper panel: Residual baseline delay mean. Both models have consistent results. Lower panel: Residual baseline delay RMS. Red dots are for Calc 9, blue for Calc 11, and grey for the difference. There are small differences, and no preference for a particular delay model is seen here. The array delay RMS is 0.3802 ns for Calc 9 (red dotted line) and 0.3829 ns for Calc 11 (blue dotted line).

Figure 5 shows that the difference between the models is small, of only -2.7 ps for the difference of the array delay RMS (Calc 9-Calc 11).

In summary we find minimal differences between the Calc delay models from the all sky tests. With slightly smaller values of the array delay RMS (by a couple of ps) for Calc 9.

5. Performance in a phase-referencing experiment

Here we compare the results for the phase-referencing part of TV010A for the two delay models in terms of the recovered offsets, flux density and source size of the target sources.

5.1. Single offset value for the whole test

We now compare the delay models using single values for the whole experiment. That is deriving a single value for all the scans. We use J2216+3518 as the phase calibrator, while J2212+3303 and J2203+3145 as targets, respectively at 2.33 and 4.47 degrees of the phase calibrator. A model map of the phase calibrator is made using self-calibration of the Calc 9 data. This model map is used to correct the phases with CALIB for both delays models. The astrometry is performed by fitting a gaussian to the source images with JMFIT (Figures 6 and 7 show the source images), using the same tight box for both delay models. The results of the astrometry for both delay models are shown in Table 1, along with their comparison.

Table 1: Phase referencing test results with Calc 9 and Calc 11. Upper and lower tables are results for the astrometry with the two delay models. The bottom table is a comparison of them. The phase calibrator is J2212+3518, and the targets J2212+3308 (2.33 degrees from phase calibrator) and J2203+3145 (4.47 degrees from phase calibrator). See the column descriptions below the table.

J2216 as phase calibrator, cellsize = 0.2 mas

CALC9						IMSTAT	IMEAN		JMFIT	Deconvolved size	
source	**dx(mas)**	**sig-dx(mas)**	**dy(mas)**	**sig-dy(mas)**	**peak (Jy/b)**	**rms (Jy/b)**	**rms (Jy/b)**	**DR**	**majax(mas)**	**minax(mas)**	**posang(deg)**
J2216	0.0012	0.0002	0.0028	0.0005	5.29E-001	2.58E-004	2.47E-004	2046	0.334	0.102	165.8
J2203	-0.4818	0.0098	0.2952	0.0168	9.15E-001	1.79E-002	1.56E-002	51	1.054	0.062	111.0
J2212	0.5270	0.0060	0.9158	0.0108	5.92E-002	5.95E-004	5.75E-004	99	0.791	0.403	62.1

CALC11						IMSTAT	IMEAN		JMFIT	Deconvolved size	
source	**dx(mas)**	**sig-dx(mas)**	**dy(mas)**	**sig-dy(mas)**	**peak (Jy/b)**	**rms (Jy/b)**	**rms (Jy/b)**	**DR**	**majax(mas)**	**minax(mas)**	**posang(deg)**
J2216	0.0012	0.0002	0.0022	0.0005	5.29E-001	2.58E-004	2.45E-004	2048	0.334	0.101	165.8
J2203	-0.4210	0.0096	0.2162	0.0165	9.15E-001	1.76E-002	1.53E-002	52	1.077	0.162	112.7
J2212	0.5514	0.0057	0.8780	0.0105	6.10E-002	5.92E-004	5.74E-004	103	0.688	0.325	60.0

Difference CALC09-CALC11								JMFIT	Deconvolved size	
Source	**Ddx(uas)**	**sigDdx(uas)**	**Ddy(uas)**	**sigDdy(uas)**	**Peak Ratio**	**RMS ratio**	**RMS ratio**	**maj ax ratio**	**min ax ratio**	**Dposang(deg)**
J2216	0.0	0.3	0.6	0.7	1.00	1.00	1.00	1.00	1.01	0.0
J2203	-60.8	13.7	79.0	23.5	1.00	1.02	1.02	0.98	0.38	-1.7
J2212	-24.4	8.2	37.8	15.0	0.97	1.01	1.00	1.15	1.24	2.1

Column descriptions. **dx(mas) and dy(mas):** offset from coordinate position in mas; **sig-dx(mas) and sig-dy(mas):** position error for the fitted gaussian component from JMFIT; **peak (Jy/b):** peak flux density in Jy per beam from JMFIT; **rms (Jy/b):** RMS of the flux density measured with IMSTAT in a region excluding the peaks and with IMEAN by fitting the histogram of flux densities; **DR:** dynamic range of the image computed using IMSTAT RMS; **majax(mas), minax(mas) and posang(deg):** de-convolved gaussian component parameters from JMFIT. Major and minor axes in mas, and position angle in degrees; **Ddx(uas) and Ddy(uas):** difference between delay model offsets in μas; **sigDdx(uas) and sigDy(uas):** error in the offset difference for the delay models. It is obtained as the squared sum of the individual positions errors of the gaussian fits to give a formal approximation to the error.

The position offset for the phase calibrator J2216+3518 provides an estimate of the minimum error we can expect, and in this case it can be up to 3 μas, and is slightly larger for Calc 9 in the y direction. The measured

offsets for the targets differ by up to about 40 μas for J2212+3303 at 2.33 degrees from the target, and up to 80 μas for J2203+3145 at 4.47 degrees from the calibrator. From the images in Figures 6 and 7, and the increased errors in the fitted positions at larger target-calibrator distances in Table 1, it is clear that the phase transfer has problems at larger distances, increasing the error in the astrometry.

In terms of the flux density ratio at peak and image RMS we find agreement at the 3% level between both models. The deconvolved sizes for the gaussian fit with JMFIT agree within a 24% for the closer target. The case of the farther target is more complicated, with an 2% agreement on the major axis and a very large difference for the minor axis probably driven by a deconvolved size smaller than fitting errors. The position angles are very similar, and differ by only a few degrees.

We also investigated possible variations of the above result on the size of the cells used in IMAGR. We tried with sizes of 0.15 and 0.25 mas and obtained similar results (see Table 2) for the relative difference between Calc 9 and Calc 11. Nonetheless, there are shifts between the offsets for a given delay model using different cell sizes. These are of up to about 10 μas when using 0.15 mas cells with respect to the results with 0.20 mas cells for both delay models. The shifts are larger when using larger 0.25 mas cells, of about 30 μas in some cases.

Table 2: Phase referencing test results with Calc 9 and Calc 11. Upper and lower tables are results for the astrometry with the two delay models. The bottom table is a comparison of them. The phase calibrator is J2212+3518, and the targets J2212+3308 (2.33 degrees from phase calibrator) and J2203+3145 (4.47 degrees from phase calibrator). The results for two different values of the cell size used in IMAGR are presented here as a way to evaluate the sensitivity of the results presented in Table 1, obtained using a 0.2 mas cell size. See the column descriptions in Table 1 .

J2216 as phase calibrator, cellsize = 0.15 mas

CALC09						IMSTAT	IMEAN		JMFIT	Deconvolved size	
source	**dx(mas)**	**sig-dx(mas)**	**dy(mas)**	**sig-dy(mas)**	**peak (Jy/b)**	**rms (Jy/b)**	**rms (Jy/b)**	**DR**	**majax(mas)**	**minax(mas)**	**posang(deg)**
J2216	0.0013	0.0002	0.0030	0.0006	5.29E-001	2.85E-004	2.95E-004	1858	0.327	0.099	167.7
J2203	-0.4827	0.0127	0.2958	0.0220	9.14E-001	1.95E-002	1.99E-002	47	1.080	0.000	20.1
J2212	0.5145	0.0074	0.9089	0.0132	5.84E-002	7.33E-004	6.83E-004	80	0.849	0.479	63.7

CALC11						IMSTAT	IMEAN		JMFIT	Deconvolved size	
source	**dx(mas)**	**sig-dx(mas)**	**dy(mas)**	**sig-dy(mas)**	**peak (Jy/b)**	**rms (Jy/b)**	**rms (Jy/b)**	**DR**	**majax(mas)**	**minax(mas)**	**posang(deg)**
J2216	0.0013	0.0002	0.0030	0.0006	5.29E-001	2.84E-004	2.94E-004	1862	0.327	0.099	167.7
J2203	-0.4158	0.0117	0.2182	0.0207	9.35E-001	1.87E-002	1.90E-002	50	1.087	0.000	24.8
J2212	0.5416	0.0070	0.8739	0.0130	6.02E-002	7.29E-004	6.93E-004	83	0.748	0.417	62.0

Difference CALC09-CALC11								JMFIT	Deconvolved size	
Source	**Ddx(uas)**	**sigDdx(uas)**	**Ddy(uas)**	**sigDdy(uas)**	**Peak Ratio**	**RMS ratio**	**RMS ratio**	**maj ax ratio**	**min ax ratio**	**Dposang(deg)**
J2216	0.0	0.3	0.0	0.8	1.00	1.00	1.00	1.00	1.00	0.0
J2203	-66.9	17.3	77.5	30.1	0.98	1.04	1.05	0.99	---	-4.7
J2212	-27.1	10.2	35.0	18.5	0.97	1.01	0.99	1.14	1.15	1.8

J2216 as phase calibrator, cellsize = 0.25 mas

CALC09						IMSTAT	IMEAN		JMFIT	Deconvolved size	
source	**dx(mas)**	**sig-dx(mas)**	**dy(mas)**	**sig-dy(mas)**	**peak (Jy/b)**	**rms (Jy/b)**	**rms (Jy/b)**	**DR**	**majax(mas)**	**minax(mas)**	**posang(deg)**
J2216	0.0015	0.0002	0.0032	0.0004	5.29E-001	2.17E-004	2.32E-004	2442	0.336	0.097	166.2
J2203	-0.4575	0.0087	0.3245	0.0134	8.97E-001	1.18E-002	1.30E-002	76	1.117	0.236	97.6
J2212	0.5007	0.0054	0.9090	0.0098	5.81E-002	5.36E-004	5.07E-004	108	0.788	0.551	60.7

CALC11						IMSTAT	IMEAN		JMFIT	Deconvolved size	
source	**dx(mas)**	**sig-dx(mas)**	**dy(mas)**	**sig-dy(mas)**	**peak (Jy/b)**	**rms (Jy/b)**	**rms (Jy/b)**	**DR**	**majax(mas)**	**minax(mas)**	**posang(deg)**
J2216	0.0012	0.0002	0.0028	0.0004	5.29E-001	2.16E-004	2.30E-004	2454	0.334	0.098	167.5
J2203	-0.4150	0.0085	0.2275	0.0133	9.14E-001	1.17E-002	1.27E-002	78	1.230	0.237	115.4
J2212	0.5292	0.0051	0.8750	0.0095	5.98E-002	5.31E-004	5.07E-004	113	0.705	0.501	52.0

Difference CALC09-CALC11								JMFIT	Deconvolved size	
Source	**Ddx(uas)**	**sigDdx(uas)**	**Ddy(uas)**	**sigDdy(uas)**	**Peak Ratio**	**RMS ratio**	**RMS ratio**	**maj ax ratio**	**min ax ratio**	**Dposang(deg)**
J2216	0.3	0.2	0.5	0.6	1.00	1.01	1.01	1.01	0.99	-1.3
J2203	-42.5	12.2	97.0	18.8	0.98	1.01	1.02	0.91	1.00	-17.8
J2212	-28.5	7.4	34.0	13.7	0.97	1.01	1.00	1.12	1.10	8.7

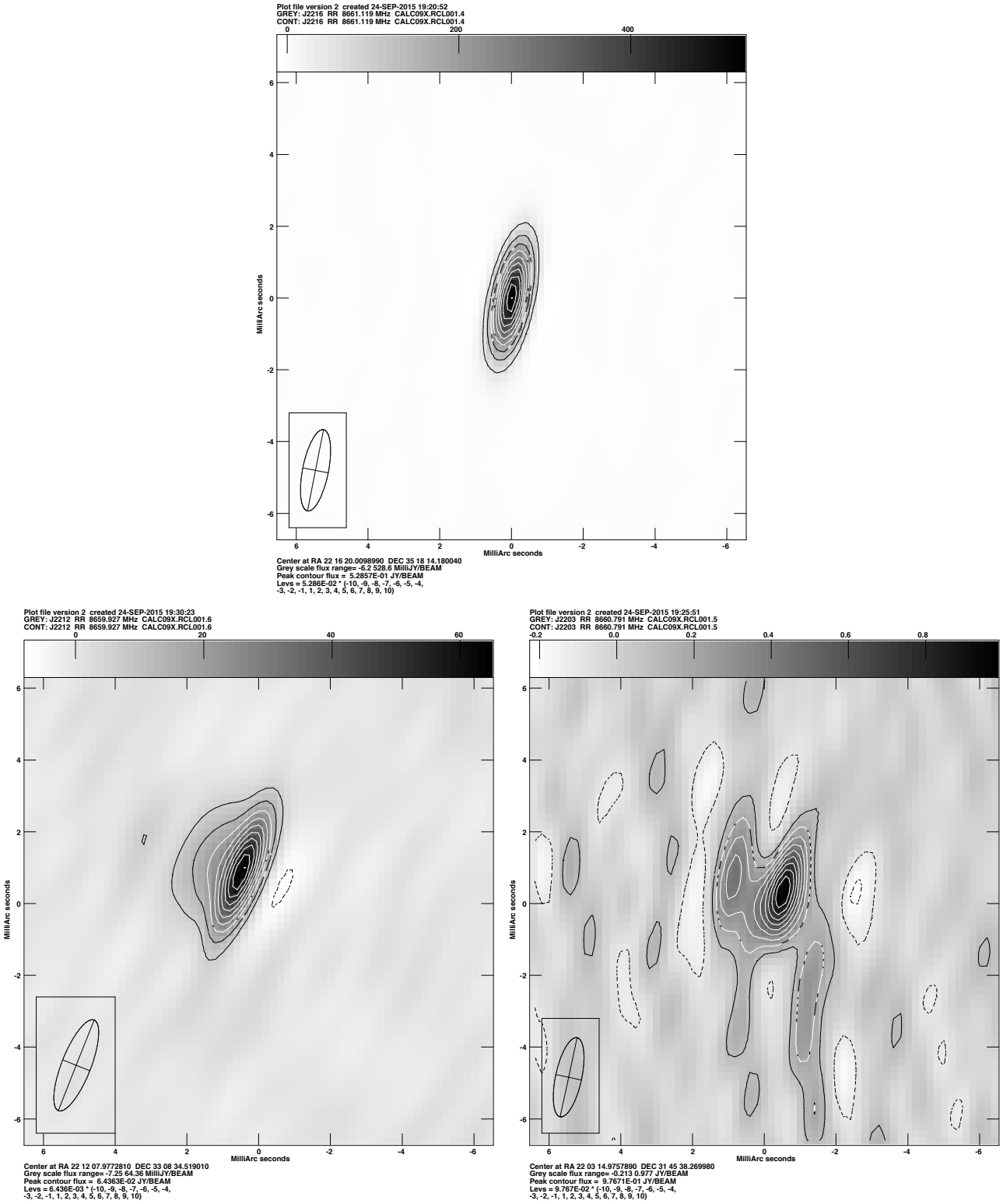

Fig. 6.— Phase referencing test with Calc 9. Upper panel: Phase calibrator J2216+3518 after self-calibration. Lower panels: Targets J2212+3308 (2.33 degrees from phase calibrator) and J2203+3145 (4.47 degrees from phase calibrator). There are clear artifacts in both images caused by the different sky positions of the sources. In all cases the cell size used is 0.2 mas.

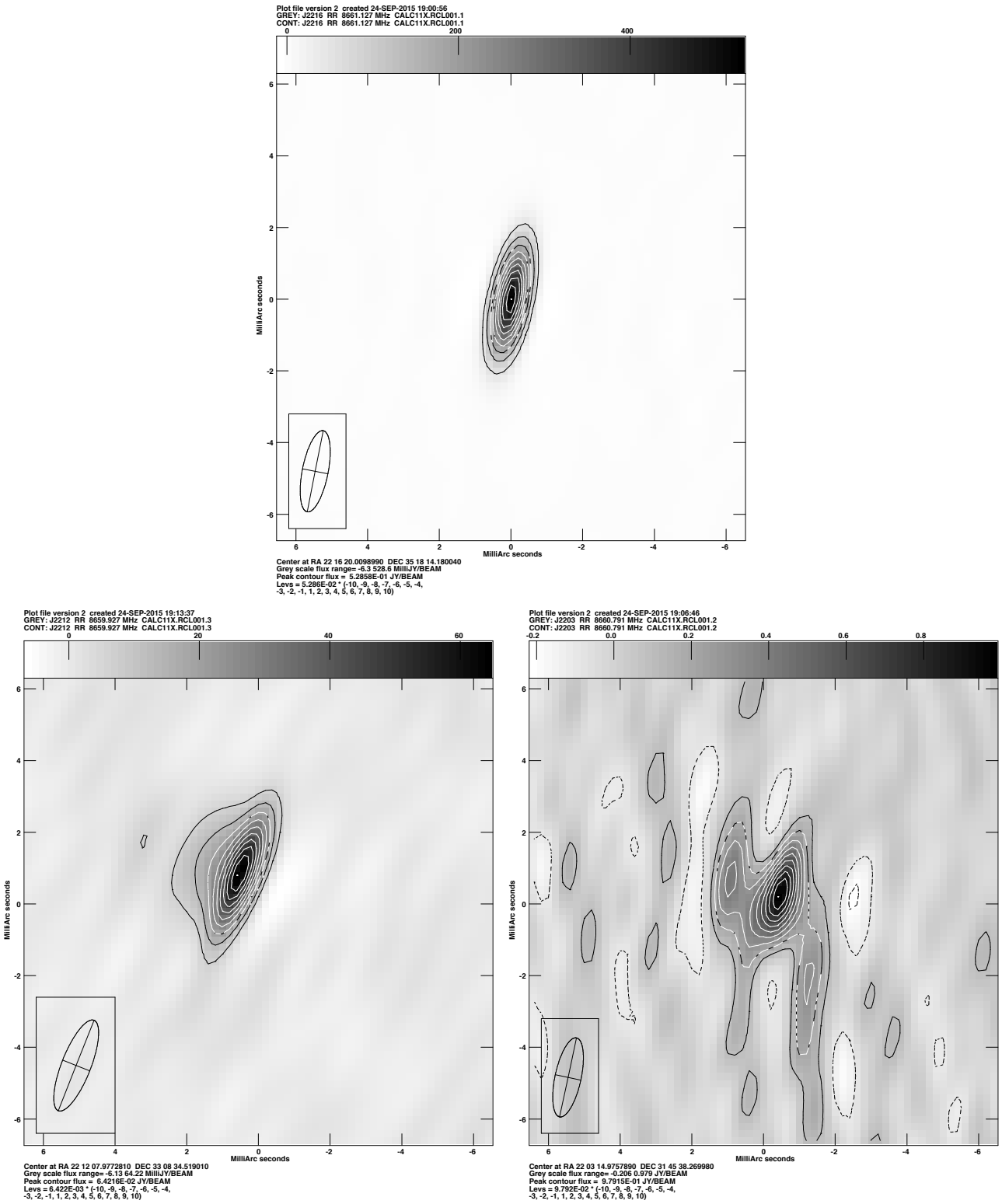

Fig. 7.— Phase referencing test with Calc 11. Upper panel: Phase calibrator J2216+3518 after self-calibration. Lower panels: Targets J2212+3308 (2.33 degrees from phase calibrator) and J2203+3145 (4.47 degrees from phase calibrator). There are clear artifacts in both images caused by the different sky positions of the sources. In all cases the cell size used is 0.2 mas.

5.2. Dividing the experiment into multiple sections

We now repeat the test describe before but dividing the experiment into three blocks. These sections are periods of continuous calibrator-target switching and can be clearly identified in Figures 1 and 2. Each section is treated independently and the results of a comparison of the consistency between the three sections are described below. Table 3 shows the results for J2212+3308 which has a distance of 2.33 degrees to the phase calibrators, and can be used as an example of what to expect in a typical science observation.

Table 3: Phase referencing test results with Calc 9 and Calc 11, for the experiment divided into three sections. Upper and lower tables are results for the astrometry with the two delay models. The bottom table is a comparison of them. The phase calibrator is J2212+3518, and only the results for J2212+3308 (2.33 degrees from phase calibrator) are presented. See the column descriptions in Table 1.

J2212+3512 offset versus time

CALC09						IMSTAT	IMEAN		JMFIT	Deconvolved size	
section	**dx(mas)**	**sig-dx(mas)**	**dy(mas)**	**sig-dy(mas)**	**peak (Jy/b)**	**rms (Jy/b)**	**rms (Jy/b)**	**DR**	**majax(mas)**	**minax(mas)**	**posang(deg)**
1	0.4396	0.0066	0.9262	0.0227	5.29E-001	4.90E-004	4.37E-004	1079	0.000	0.000	166.1
2	0.3642	0.0057	0.9942	0.0127	8.29E-001	3.28E-002	2.72E-002	25	0.002	0.000	105.1
3	0.5664	0.0268	0.9372	0.0311	3.90E-002	1.34E-003	1.11E-003	29	0.002	0.001	107.9

CALC11						IMSTAT	IMEAN		JMFIT	Deconvolved size	
section	**dx(mas)**	**sig-dx(mas)**	**dy(mas)**	**sig-dy(mas)**	**peak (Jy/b)**	**rms (Jy/b)**	**rms (Jy/b)**	**DR**	**majax(mas)**	**minax(mas)**	**posang(deg)**
1	0.4568	0.0065	0.9160	0.0227	5.29E-001	4.90E-004	4.37E-004	1080	0.000	0.000	166.1
2	0.3842	0.0056	0.9752	0.0125	8.28E-001	3.19E-002	2.67E-002	26	0.002	0.000	107.7
3	0.5868	0.0258	0.9216	0.0306	3.97E-002	1.32E-003	1.10E-003	30	0.002	0.001	112.8

Difference CALC09-CALC11								JMFIT	Deconvolved size	
	Ddx(uas)	**sigDdx(uas)**	**Ddy(uas)**	**sigDdy(uas)**	**Peak Ratio**	**RMS ratio**	**RMS ratio**	**maj ax ratio**	**min ax ratio**	**Dposang(deg)**
1	-17.2	9.2	10.2	32.1	1.00	1.00	1.00	1.00	1.00	0.0
2	-20.0	8.0	19.0	17.8	1.00	1.03	1.02	0.98	0.00	-2.7
3	-20.4	37.2	15.6	43.6	0.98	1.01	1.01	0.99	1.02	-4.9

For J2212+3308 the difference between Calc 9 and Calc 11 amounts to up to about 20 μas in position offset, 2% in flux density peak and 3% in flux density RMS. Much larger differences are observed for the target at 4.47 degrees from the phase-calibrator, with up to 70 μas in position offset, 38% in flux density peak and 15% in flux density RMS.

6. Performance comparison for Mars orbiters

To test the implementation of near-field effects, and possible differences between the two delay models we performed observations of the MRO and Odyssey. The procedure is similar as in Max-Moerbeck et al. (2015), although in this case we observed a 32 MHz bandwidth and used the standard path to correlate the data. In each case only the channels containing about 25% of the peak signal from the spacecraft tone are used in the imaging of the phase-calibrator and spacecraft. This corresponds to 1.8 MHz and 300 kHz, for the MRO and Odyssey respectively. The results of these observations are presented in Tables 4 and 5.

The position of the phase calibrator is slightly different from zero offset when using the channels for MRO and consistent with zero offset when using the channels for Odyssey. For the MRO the offsets between delay models differ by up to about 13 μas, but the fitting errors are larger, so no difference is found. The same is observed for the Odyssey, with position offsets of up to 22 μas. In terms of peak flux density and RMS, the agreement is better than 6% in all cases.

Table 4: Phase referencing test results for the MRO with Calc 9 and Calc 11. Upper and middle tables are results for the astrometry with the two delay models, and the bottom table shows a comparison of them. The target/phase-calibrator distance is 1.57 degrees. See the column descriptions in Table 1.

J2259-0811 as phase calibrator, cellsize = 0.2 mas

CALC9						IMSTAT	IMEAN	
source	**dx(mas)**	**sig-dx(mas)**	**dy(mas)**	**sig-dy(mas)**	**peak (Jy/b)**	**rms (Jy/b)**	**rms (Jy/b)**	**DR**
J2259-0811	0.0386	0.0189	-0.1458	0.0466	1.50E-001	8.70E-003	8.55E-003	17
MRO	14.8842	0.0265	-38.2636	0.0754	1.52E+002	1.39E+001	1.23E+001	11

CALC11						IMSTAT	IMEAN	
source	**dx(mas)**	**sig-dx(mas)**	**dy(mas)**	**sig-dy(mas)**	**peak (Jy/b)**	**rms (Jy/b)**	**rms (Jy/b)**	**DR**
J2259-0811	0.0372	0.0190	-0.1182	0.0483	1.55E-001	9.06E-003	9.03E-003	17
MRO	14.8970	0.0270	-38.2638	0.0754	1.62E+002	1.47E+001	1.31E+001	11

Difference CALC09-CALC11							
Source	**Ddx(uas)**	**sigDdx(uas)**	**Ddy(uas)**	**sigDdy(uas)**	**Peak Ratio**	**RMS ratio**	**RMS ratio**
J2259-0811	1.4	26.8	-27.6	67.2	0.97	0.96	0.95
MRO	-12.8	37.8	0.2	106.6	0.94	0.95	0.94

6.1. Independent estimate for the offset error

One point to notice is that the fitting errors might be overestimating the error in the astrometry. In principle the measured offset should be invariant to shifts in the image plane, in particular when these are smaller than the synthesized beam. These changes are expected when comparing the two delay models, thus an estimate of their magnitude can provide a good approximation of errors coming from this effect. We can test the repeatability of the offset measurement by producing estimates with slightly different offsets in RA and DEC. Since adding an offset in RA and DEC should not change the result, the observed changes provide an estimate for the error in the

Table 5: Phase referencing test results for the Odyssey with Calc 9 and Calc 11. Upper and middle tables are results for the astrometry with the two delay models, and the bottom table shows a comparison of them The target/phase-calibrator distance is 1.57 degrees. See the column descriptions in Table 1.

J2259-0811 as phase calibrator, cellsize = 0.2 mas

CALC9 source	dx(mas)	sig-dx(mas)	dy(mas)	sig-dy(mas)	peak (Jy/b)	IMSTAT rms (Jy/b)	IMEAN rms (Jy/b)	DR
J2259-0811	-0.0046	0.0229	-0.0278	0.0560	1.65E-001	1.13E-002	1.24E-002	15
ODY	3.2410	0.0218	-9.3792	0.0562	5.52E+001	3.89E+000	4.16E+000	14

CALC11 source	dx(mas)	sig-dx(mas)	dy(mas)	sig-dy(mas)	peak (Jy/b)	IMSTAT rms (Jy/b)	IMEAN rms (Jy/b)	DR
J2259-0811	-0.0042	0.0229	-0.0216	0.0584	1.64E-001	1.14E-002	1.24E-002	14
ODY	3.2546	0.0237	-9.3572	0.0598	5.33E+001	3.96E+000	4.32E+000	13

Difference CALC09-CALC11 Source	Ddx(uas)	sigDdx(uas)	Ddy(uas)	sigDdy(uas)	Peak Ratio	RMS ratio	RMS ratio
J2259-0811	-0.4	32.4	-6.2	80.9	1.00	0.99	0.99
ODY	-13.6	32.2	-22.0	82.0	1.03	0.98	0.96

measured position, that is independent of the error reported by JMFIT that we have used so far.

We tried three different offsets for the MRO, all with the same RA and DEC offset, just to simplify the test. We assumed a beam HPBW using the formula on the OSS[4], which gives 0.85 mas for the longest baseline. We used 1/10, 1/3 and 1/2 of the HPBW, which is 0.09, 0.28 and 0.43 mas. Since the measured offsets from JMFIT are now computed from a different phase center, we used the fitted gaussian component RA and DEC reported in JMFIT, and computed relative offsets from that. In all cases we took the no-offset case as reference.

For the delay models the delay offsets RMS obtained with this test for the x and y directions are:

Calc 9:

$$x_{\rm RMS} = 5.0\ \mu{\rm as}$$
$$y_{\rm RMS} = 24.9\ \mu{\rm as}$$

Calc 11:

$$x_{\rm RMS} = 5.7\ \mu{\rm as}$$
$$y_{\rm RMS} = 18.8\ \mu{\rm as}.$$

These errors are smaller, by up to a factor of 4, than the errors reported for MRO by JMFIT in Table 5. With these errors we get for the difference of the offsets between Calc 9 and Calc 11

[4] https://science.nrao.edu/facilities/vlba/docs/manuals/oss/ang-res

$$\Delta x_{\rm off} = -13.6 \pm 7.6 \ \mu{\rm as}$$
$$\Delta y_{\rm off} = -22.0 \pm 31.2 \ \mu{\rm as}.$$

Indicating comparatively larger differences, whith respect to what is found using the fitting errors from JMFIT. This suggest that there could be differences between the two models of about 10-20 μas that need to be investigated carefully for long term projects using data from both models.

7. Conclusions

The two delay models produce similar results for the raw delays (Section 3), the residual delays obtained from fringe fitting (Section 4) and their performance in a phase-referencing experiment (Sections 5.1 and 5.2). Nonetheless, there are small observed differences that are summarized below.

A comparison of the raw delays for each one (Section 3) shows differences of less than 100 ps, with typical values of a few tens of ps.

The all-sky test (Section 4) also shows comparable results, with slightly smaller values of the residual delay RMS for Calc 9 by about a couple of ps.

The phase-referencing experiment of Section 5.1 shows differences between the offsets measured by the two delay models of up to about 40 μas for a 2.33 degrees target-calibrator distance and up to 80 μas when that distance is 4.47 degrees. When the experiment is divided in to three blocks (Section 5.2), the differences are of up to about 20 μas for a 2.33 degrees target-calibrator distance and up to 70 μas when that distance is 4.47 degrees.

The astrometry in the Mars orbiters provided similar results for the two delay models, with differences of up to about 22 μas.

These differences could affect long term projects using both delay models and careful consideration of them by the users will be needed in those cases.

Acknowledgements

We thank Vivek Dhawan, Amy Mioduszewski, Jonathan Romney, John Benson and Barry Clark for useful comments and suggestions.

REFERENCES

Deller, A. T., Tingay, S. J., Bailes, M., & West, C. 2007, PASP, 119, 318

Max-Moerbeck, W., Brisken, W. F., & Romney, J. D. 2015, PASP, 127, 161